

RESEARCH ARTICLE

10.1002/2017JA024470

Key Points:

- The disappearance of plasmaspheric hiss resulted from the removal of dayside chorus
- The temporary recovery of plasmaspheric hiss was produced by the enhancement of local instability
- The substantial recovery of plasmaspheric hiss was caused by the combination of chorus recurrence and local instability enhancement

Supporting Information:

- Supporting Information S1

Correspondence to:

Z. Su,
szpe@mail.ustc.edu.cn

Citation:

Liu, N., Su, Z., Gao, Z., Reeves, G. D., Zheng, H., Wang, Y., & Wang, S. (2017). Shock-induced disappearance and subsequent recovery of plasmaspheric hiss: Coordinated observations of RBSP, THEMIS, and POES satellites. *Journal of Geophysical Research: Space Physics*, 122. <https://doi.org/10.1002/2017JA024470>

Received 13 JUN 2017

Accepted 27 SEP 2017

Accepted article online 4 OCT 2017

Shock-Induced Disappearance and Subsequent Recovery of Plasmaspheric Hiss: Coordinated Observations of RBSP, THEMIS, and POES Satellites

Nigang Liu^{1,2,3} , Zhenpeng Su^{1,2} , Zhonglei Gao^{1,2,3} , G. D. Reeves^{4,5} , Huinan Zheng^{1,2} , Yuming Wang¹ , and Shui Wang¹

¹CAS Key Laboratory of Geospace Environment, Department of Geophysics and Planetary Sciences, University of Science and Technology of China, Hefei, China, ²Collaborative Innovation Center of Astronautical Science and Technology, Hefei, China, ³Mengcheng National Geophysical Observatory, School of Earth and Space Sciences, University of Science and Technology of China, Hefei, China, ⁴Space Science and Applications Group, Los Alamos National Laboratory, Los Alamos, NM, USA, ⁵Space Sciences Division, New Mexico Consortium, Los Alamos, NM, USA

Abstract Plasmaspheric hiss is an extremely low frequency whistler-mode emission contributing significantly to the loss of radiation belt electrons. There are two main competing mechanisms for the generation of plasmaspheric hiss: excitation by local instability in the outer plasmasphere and origination from chorus outside the plasmasphere. Here on the basis of the analysis of an event of shock-induced disappearance and subsequent recovery of plasmaspheric hiss observed by RBSP, THEMIS, and POES missions, we attempt to identify its dominant generation mechanism. In the preshock plasmasphere, the local electron instability was relatively weak and the hiss waves with bidirectional Poynting fluxes mainly originated from the dayside chorus waves. On arrival of the shock, the removal of preexisting dayside chorus and the insignificant variation of low-frequency wave instability caused the prompt disappearance of hiss waves. In the next few hours, the local instability in the plasmasphere was greatly enhanced due to the substorm injection of hot electrons. The enhancement of local instability likely played a dominant role in the temporary recovery of hiss with unidirectional Poynting fluxes. These temporarily recovered hiss waves were generated near the equator and then propagated toward higher latitudes. In contrast, both the enhancement of local instability and the recurrence of prenoon chorus contributed to the substantial recovery of hiss with bidirectional Poynting fluxes.

1. Introduction

Plasmaspheric hiss is an extremely low frequency (~0.1 kHz to several kHz) whistler-mode emission in the terrestrial plasmasphere and plasmaspheric plumes (Hayakawa & Sazhin, 1992; Meredith et al., 2004; Russell et al., 1969; Summers et al., 2008; Thorne et al., 1973). Plasmaspheric hiss can cause the radiation belt electron losses over a wide energy range from ~0.1 MeV to several MeV through cyclotron resonant pitch angle scattering (Horne & Thorne, 1998; Summers et al., 1998). This physical process is specifically responsible for the formation of the slot region separating the inner and outer radiation belts during quiet times (e.g., Abel and Thorne, 1998; Albert, 1994; He et al., 2016; Lyons and Thorne, 1973; Meredith et al., 2007; Thorne et al., 2013) and the precipitation loss of outer radiation belt electrons during geomagnetically active times (e.g., Li et al., 2007; Mourenas and Ripoll, 2012; Ni et al., 2014; Shprits et al., 2009; Su et al., 2011, 2016; Thorne et al., 2013).

The generation mechanism of plasmaspheric hiss is of great interest in the radiation belt community. Generally, the main candidate mechanisms can be categorized into (1) generation by a local instability inside the plasmasphere and (2) origination from an embryonic source (a remote instability outside the plasmasphere or a remote source that injects waves into the plasmasphere). Early theory (Cornilleau-Wehrlin et al., 1993; Solomon et al., 1988; Thorne et al., 1979) suggested the excitation of hiss waves by the cyclotron instability of energetic electrons in the outer plasmasphere. Huang et al. (1983) and Church and Thorne (1983) thought that the gain from the local instability was too low to explain the typical hiss intensity without an embryonic source. Sonwalkar and Inan (1989), Draganov et al. (1992), and Green et al. (2005) attributed the embryonic source of plasmaspheric hiss to the lightning-generated whistlers. Ray-tracing simulations (Bortnik, Chen, Li, Thorne, Horne, 2011; Bortnik, Chen, Li, Thorne, Meredith, et al., 2011; Bortnik et al., 2008)

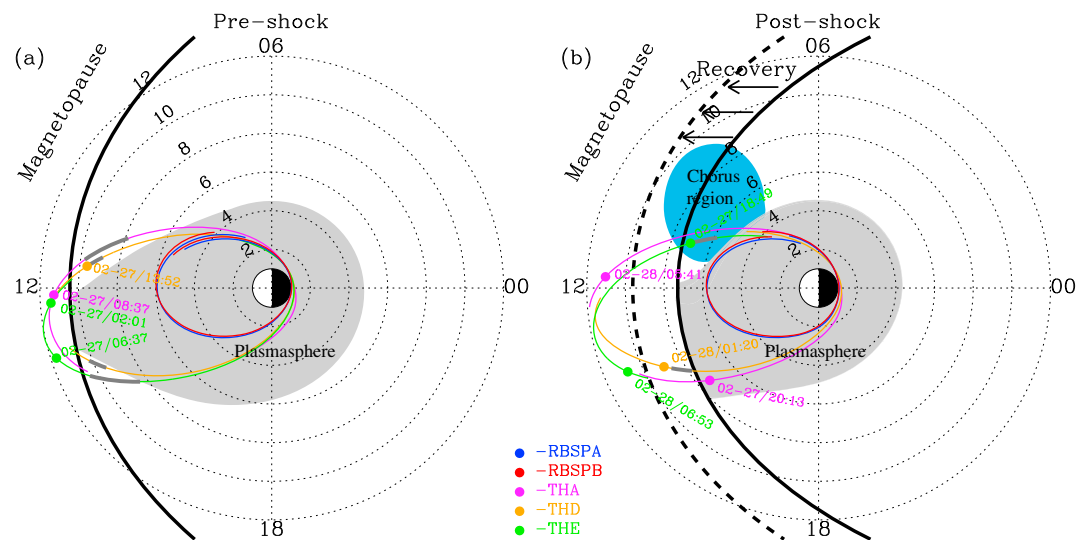


Figure 1. Schematic diagrams of magnetospheric structures and waves (a) before and (b) after the interplanetary shock. The color lines represent the orbits of RBSP and THEMIS satellites in the time range of interest. On the THEMIS orbits, the dots denote the observed locations of magnetopause and the gray segments denote the spatial ranges with observable chorus waves. The blue shadow in Figure 1b marks the spatial region with intense chorus waves estimated from the POES-observed precipitating electron fluxes after the shock.

and observations (Bortnik et al., 2009; Li et al., 2015; Meredith et al., 2013) linked the origin of plasmaspheric hiss to the whistler-mode chorus outside the plasmasphere. Subsequently, the detailed ray-tracing simulations (Chen, Bortnik, et al., 2012a, 2012b; Chen, Li, et al., 2012) suggested that the combination of embryonic source and internal amplification were required to account for the spectral intensity of dayside plasmaspheric hiss. For the unusual low-frequency hiss (Li, Thorne, et al., 2013), the repeated amplification during the cyclic ray paths in the unstable region was considered the dominant mechanism (Chen, Thorne, et al., 2014). Recently, some observations (Kletzing et al., 2014; Laakso et al., 2015) on wave Poynting fluxes indicated that the hiss waves originated from the equatorial region of the outer plasmasphere or the plasmaspheric plume. The coherent hiss waves with complex fine structures have been reported (Summers et al., 2014), which have been interpreted as a result of the nonlinear cyclotron resonance in the plasmasphere (Omura et al., 2015).

The solar wind disturbances can cause the prompt variations of magnetospheric waves and particles (Liu et al., 2017; Su et al., 2015), providing a new opportunity to examine the generation mechanism of plasmaspheric hiss. Su et al. (2015) presented the first report of disappearance of plasmaspheric hiss triggered by an interplanetary shock, but the detailed physical process remained unclear because of the lack of simultaneous wave/particle observations inside and outside the plasmasphere. Here we investigate the shock-induced disappearance and subsequent recovery of plasmaspheric hiss using the coordinated observations of the Van Allen Probes (RBSP) (Mauk et al., 2013), the Time History of Events and Macroscale Interactions during Substorm (THEMIS) satellites (Angelopoulos, 2008), and the Polar Orbiting Environmental Satellites (POES) (Dittberner, 2002) on 27 February 2014. These multipoint observations both inside and outside the plasmasphere allow a deep understanding of the generation process of plasmaspheric hiss.

2. Data and Instrumentation

In this event, the magnetosphere was well monitored by the RBSP, THEMIS, and POES missions. RBSP mission contained two satellites which had the highly elliptical orbits with perigees about $0.1 R_E$ and apogees about $6 R_E$. Three THEMIS satellites (THEMIS A, THEMIS D, and THEMIS E) in near-equatorial orbits with apogees above $10 R_E$ and perigees below $2 R_E$ were monitoring the near-Earth magnetosphere. The POES satellites had the low Earth orbits with altitudes of $\sim 0.1 R_E$, and in the time period of interest, NOAA 15, NOAA 16, NOAA 18, NOAA 19, METOP-1, and METOP-2 were operating.

The RBSP mission mainly observed fields, waves, and particles inside the plasmasphere. The electromagnetic fields were measured by the Electric Field and Waves (EFW) (Wygant et al., 2013) instrument and by the triaxial

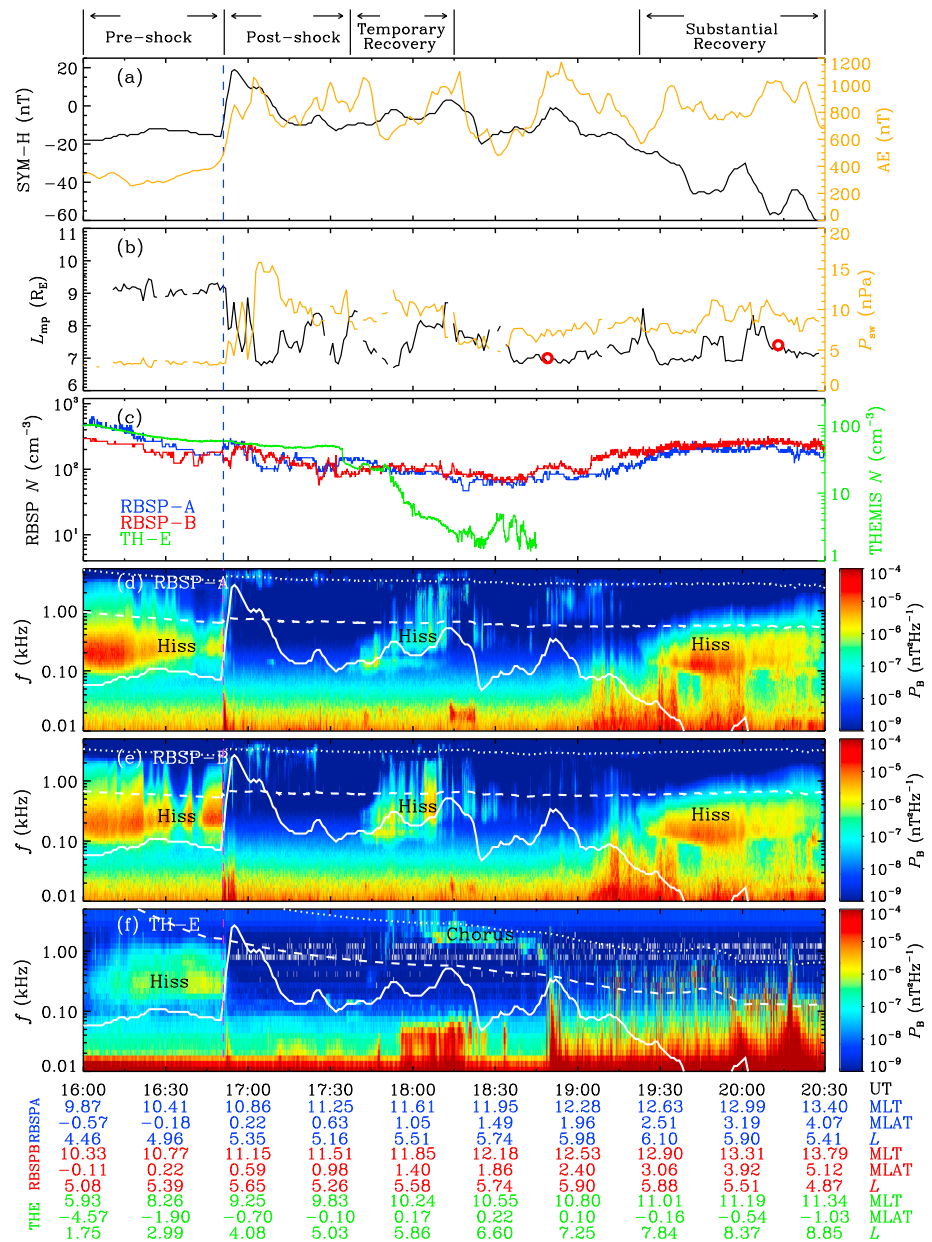


Figure 2. Overview of the plasmaspheric hiss event: (a) geomagnetic activity indices; (b) solar wind dynamic pressure and subsolar magnetopause location from the statistical model (line) and the THEMIS observations (red circles); (c) cold electron densities measured by RBSP A, RBSP B, and THEMIS E satellites; (d–f) magnetic field power spectral intensities observed by RBSP A, RBSP B, and THEMIS E satellites. The vertical dashed line marks the arrival time of the interplanetary shock. In Figures 2d–2f, the solid white lines represent the SYM-H indices, and the dashed and dotted lines represent $0.1f_{ce_eq}$ and $0.5f_{ce_eq}$.

fluxgate magnetometer (MAG) of the Electric and Magnetic Field Instrument Suite and Integrated Science (EMFISIS) suite (Kletzing et al., 2013). The wave spectral matrices in the frequency range of 0.01–5 kHz were provided by the Waveform Receiver (WFR) of the EMFISIS Waves instrument, and the singular value decomposition (SVD) method (Santolík et al., 2003, 2014) was used to determine the wave propagation characteristics (wave normal angle, ellipticity, planarity, and Poynting flux). The cold electron densities were derived from the upper hybrid resonance frequency measured by the High-Frequency Receiver (HFR) of the EMFISIS Waves instrument. The suprathermal and energetic electrons were detected by the Helium Oxygen Proton Electron (HOPE) Mass Spectrometer (Funsten et al., 2013) and the Magnetic Electron Ion Spectrometer (MagEIS) (Blake et al., 2013) of the Energetic Particle, Composition, and Thermal Plasma (ECT) Suite (Spence et al., 2013).

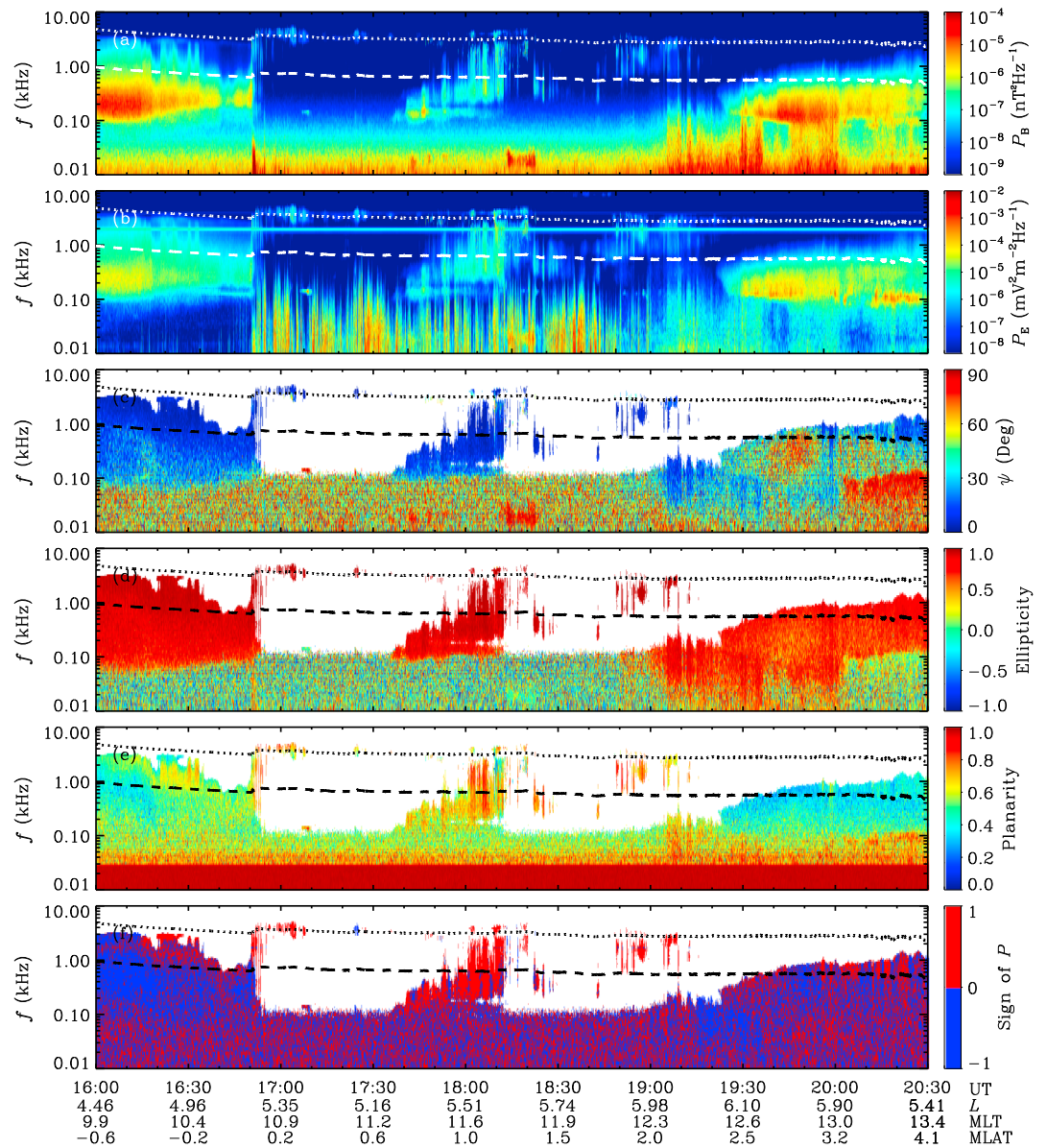


Figure 3. Wave propagation characteristics measured by RBSP A satellite: (a and b) magnetic and electric field power spectral densities; (c) wave normal angle; (d) ellipticity; (e) planarity; (f) sign of parallel Poynting fluxes. The dashed and dotted lines represent $0.1f_{ce_eq}$ and $0.5f_{ce_eq}$.

The THEMIS mission observed fields, waves, and particles both inside and outside the plasmasphere. The electromagnetic fields were detected by the Fluxgate Magnetometer (FGM) (Auster et al., 2008) and the Electric Field Instrument (EFI) (Bonnell et al., 2008). The wave power spectra densities in the frequency range of 0.01–5 kHz were observed by the Search Coil Magnetometer (SCM) (Le Contel et al., 2008). The suprathermal and energetic electron fluxes were observed by the Electrostatic Analyzer (ESA) (McFadden et al., 2008) and the Solid State Telescope (SST) (Angelopoulos, 2008). The cold electron densities were estimated from the spacecraft potential and the electron thermal speed (Li et al., 2010) measured by EFI and ESA.

According to the theory established by Stix (1962), Cornwall (1964), and Kennel and Petschek (1966), the whistler-mode chorus waves can efficiently scatter the low-energy electrons into the loss cone (e.g., Lam et al., 2010; Meredith et al., 2011). The Medium Energy Proton and Electron Detector (MEPED) of the POES mission detected the precipitating electron fluxes in the energy range of 30–2500 keV. These electron fluxes had been

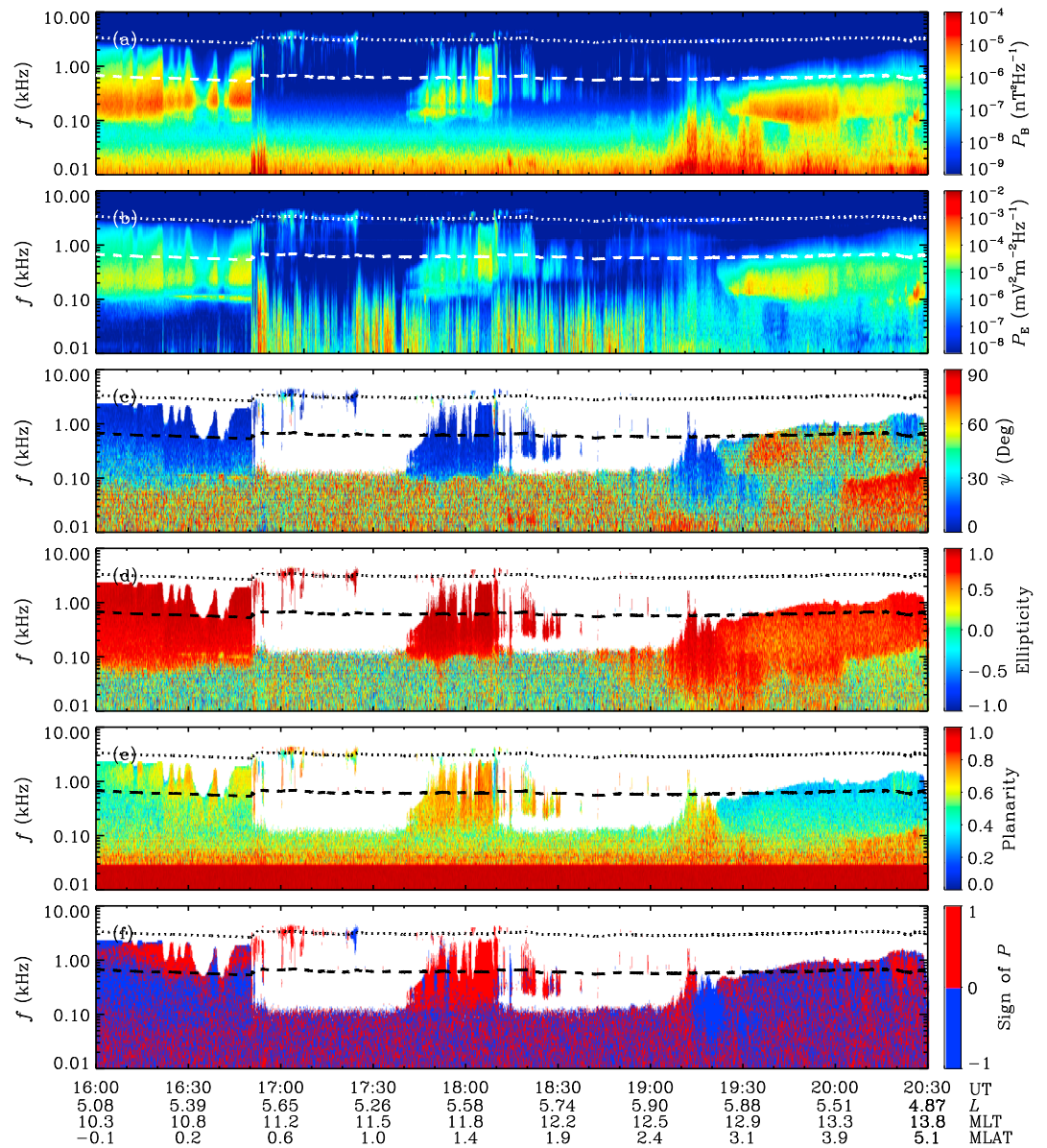


Figure 4. Same as Figure 3, except for RBSP B satellite.

shown to be positively correlated with the chorus wave intensities in the magnetosphere (Chen, Reeves, et al., 2014; Li, Ni, et al., 2013). The POES observations over a broad region in *L*-shell and magnetic local time (MLT) allowed one to evaluate the global distributions of chorus waves.

The interplanetary parameters and geomagnetic activity indices are taken from the OMNI database of CDAWeb (King & Papitashvili, 2005). The subsolar magnetopause location is determined from the interplanetary parameters on the basis of the previous statistical model (Lin et al., 2010). The global plasmapause location is roughly determined on the basis of the available density observations and the numerical simulations of Goldstein et al. (2014). The equatorial magnetic fields are obtained from $B_{eq} = B_o B_{Me}/B_{Mo}$, with the locally observed magnetic fields B_o , and the ratio B_{Me}/B_{Mo} of equatorial magnetic fields to local magnetic fields in the TS04 field model (Tsyganenko & Sitnov, 2005).

3. Event Overview

Figures 1 and 2 show an overview of the plasmaspheric hiss evolution event on 27 February 2014. The apogees of RBSP and THEMIS satellites were near the local noon sector of the magnetosphere. Before the interplanetary

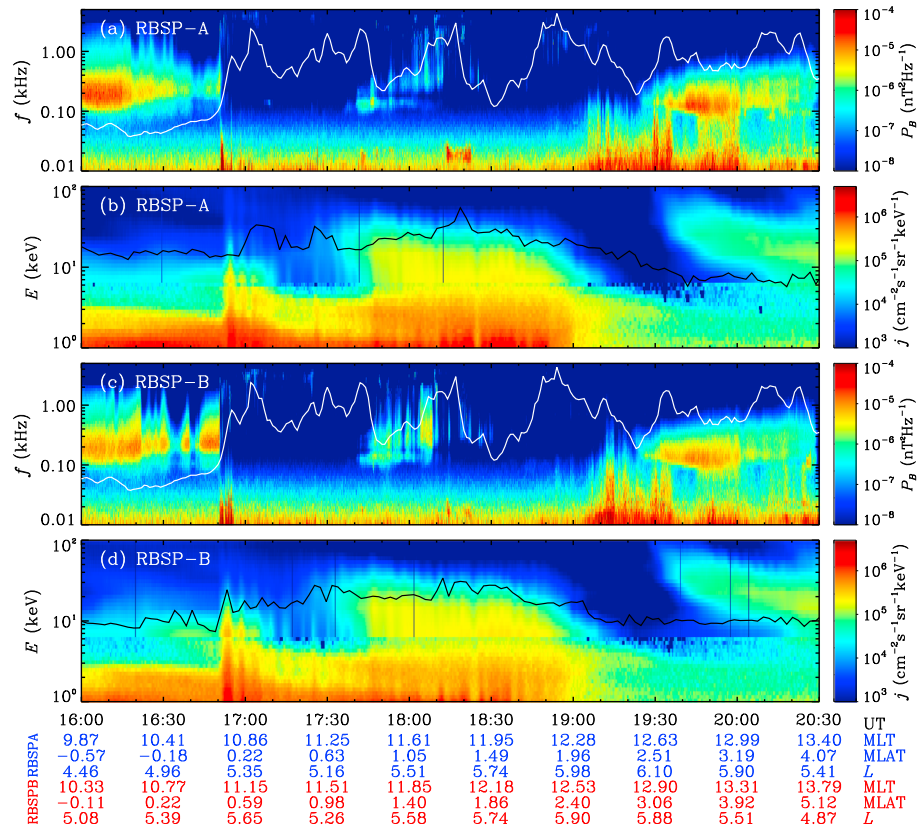


Figure 5. Wave intensities and hot electron distributions measured by twin RBSP satellites in the time range from 16:00 UT to 20:30 UT. The white lines in Figures 5a and 5c represent the AE indices, while the black lines in Figures 5b and 5d represent the minimum resonant energies of 0.3 kHz whistler-mode waves.

shock arrival, the subsolar magnetopause varied in the vicinity of $10 R_E$ (Earth radii) depending on the specific solar wind conditions. The core plasmasphere was confined to $<4.5 R_E$, and the plasmaspheric plume extending toward the dayside magnetopause formed in the time period from 03:00 UT to 06:00 UT on 27 February 2014 (Goldstein et al., 2014). Around 16:50 UT, an interplanetary shock hit the magnetosphere and directly caused an earthward movement of the subsolar magnetopause by $2 R_E$ and a sudden increase of *SYM-H* index from -15 nT to 20 nT. During the passage of the shock sheath and the associated interplanetary coronal mass ejection, the magnetosphere experienced a moderate storm (with the minimum *SYM-H* of >-100 nT) and some prolonged substorms (with the maximum *AE* of 1100 nT). As observed by RBSP A, RBSP B, and THEMIS E satellites inside the high-density plasmasphere/plume, the shock caused the disappearance of plasmaspheric hiss waves in the frequency range from 0.1 kHz to 1.0 kHz and the emergence of weak waves above 1 kHz (approximately corresponding to $0.5 f_{ce_eq}$, with the equatorial electron gyrofrequency f_{ce_eq}). Approximately 1 h after the shock arrival, a temporary recovery of plasmaspheric hiss waves occurred in the same frequency range (0.1–1.0 kHz) at the locations ($L \sim 5.5$, *MLT* ~ 11.7) of twin RBSP satellites. Almost at the same time, THEMIS E detected an impulsive enhancement of chorus waves in the frequency range above 1 kHz outside the plasmasphere ($L \sim 6$, *MLT* ~ 10.3). After 18:49 UT, THEMIS E went outside the magnetopause. After 19:30 UT, as observed by the twin RBSP satellites, the hiss waves recovered substantially from the influence of the interplanetary shock.

4. Wave Propagation Characteristics

Figures 3 and 4 present the wave propagation characteristics derived from the twin RBSP observations on 27 February 2014. In the time period of interest, the observed waves above 0.1 kHz were mainly whistler-mode emissions with the ellipticity values close to 1. The temporarily recovered hiss waves (from 17:40 UT to 18:15 UT) had the largest values (>0.7) of planarity, followed by the preshock hiss (0.5–0.7). The substantially

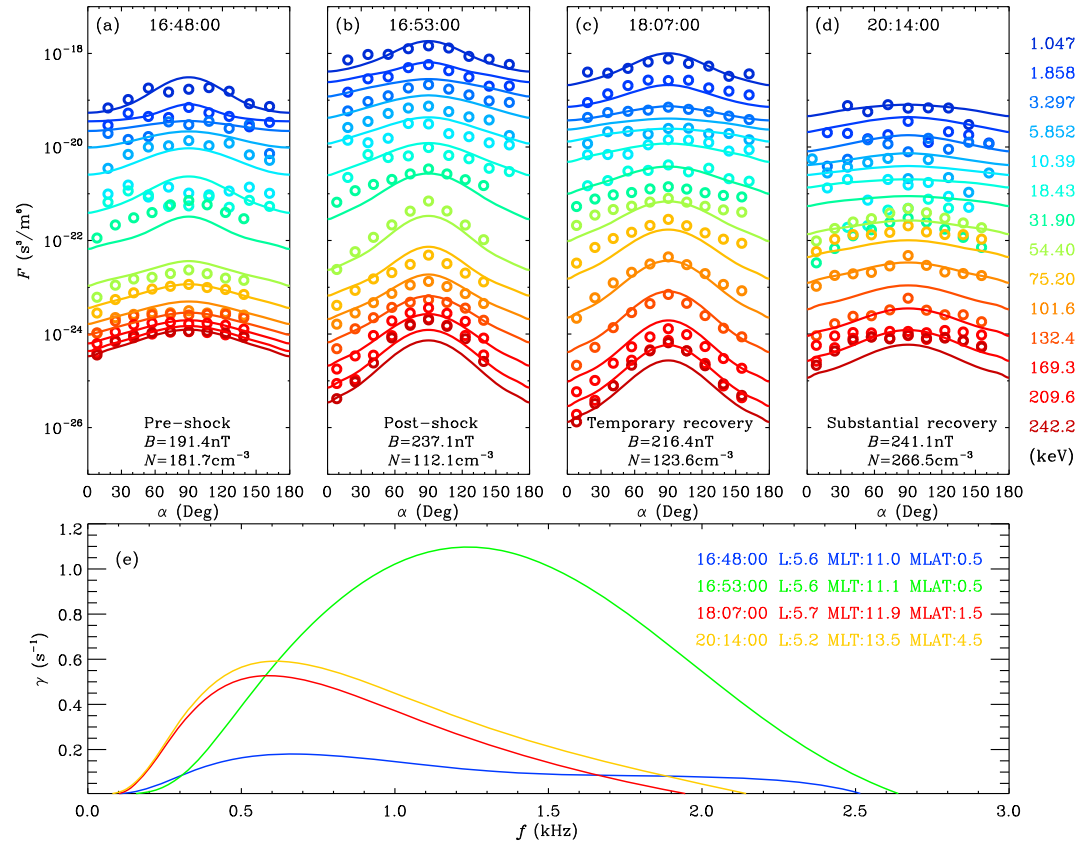


Figure 7. Evaluation of local instabilities of hot electrons: (a–d) observed (circles) and modeled (lines) energetic electron phase space densities of RBSP B at four indicated times; (e) linear growth rates of parallel-propagating whistler waves (color coded according to time).

Table 1
Four Groups of Fitting Parameters for Electron PSDs in the Energy Range of 1–300 keV

| Groups | Components | $n_i(m^{-3})$ | T_i (keV) | Δ_i | α_{1_i} | α_{2_i} | V_{dr_i} |
|--|------------|----------------------|-------------|------------|----------------|----------------|------------|
| Preshock moment at 16:48 UT | 1 | 1.0000×10^6 | 0.0256 | 0.8000 | 1.3611 | 0.2722 | 0 |
| | 2 | 2.0000×10^4 | 0.1819 | 0.7900 | 2.2500 | 0.4500 | 0 |
| | 3 | 2.0000×10^4 | 2.9112 | 1.0000 | 1.7227 | 0.3445 | 0 |
| | 4 | 1.0000×10^3 | 7.1075 | 0.8000 | 1.0816 | 0.1081 | 0 |
| | 5 | 1.5000×10^3 | 9.5639 | 0.8000 | 1.2559 | 0.1256 | 0 |
| | 6 | 1.6000×10^2 | 43.012 | 0.8000 | 1.4872 | 0.1487 | 0 |
| Postshock moment at 16:53 UT | 1 | 1.8000×10^5 | 0.0256 | 0.8000 | 1.0000 | 0.1000 | 0 |
| | 2 | 1.1800×10^5 | 0.0256 | 0.9000 | 4.0000 | 0.8000 | 0 |
| | 3 | 9.1000×10^4 | 0.1865 | 0.8000 | 2.3815 | 0.2382 | 0 |
| | 4 | 8.8000×10^4 | 1.6376 | 0.8000 | 1.5625 | 0.1563 | 0 |
| | 5 | 6.4000×10^4 | 5.0151 | 0.8000 | 1.5924 | 0.1592 | 0 |
| | 6 | 1.5000×10^3 | 14.738 | 0.8000 | 1.4267 | 0.1427 | 0 |
| Temporary recovery moment at 18:07 UT | 1 | 3.3100×10^5 | 0.0576 | 0.8000 | 1.4938 | 0.1494 | 0 |
| | 2 | 1.9000×10^5 | 0.1201 | 0.8000 | 1.7101 | 0.1710 | 0 |
| | 3 | 3.0000×10^4 | 0.3440 | 0.8000 | 1.6198 | 0.1619 | 0 |
| | 4 | 1.0000×10^4 | 0.8216 | 1.0000 | 1.6747 | 0.1675 | 0 |
| | 5 | 6.5000×10^4 | 7.3947 | 0.8000 | 1.3841 | 0.1384 | 0 |
| | 6 | 6.5000×10^2 | 14.331 | 0.8000 | 1.3338 | 0.1333 | 0 |

Table 1 (continued)

| Groups | Components | $n_i(m^{-3})$ | T_i (keV) | Δ_i | α_{1i} | α_{2i} | V_{dri} |
|---|------------|----------------------|-------------|------------|---------------|---------------|-----------|
| Substantial recovery moment at 20:14 UT | 1 | 2.1000×10^4 | 0.0114 | 0.8000 | 1.5625 | 0.1563 | 0 |
| | 2 | 6.0000×10^3 | 0.7740 | 0.8000 | 1.3967 | 0.1397 | 0 |
| | 3 | 2.1000×10^3 | 2.2289 | 0.8000 | 1.6531 | 0.1653 | 0 |
| | 4 | 3.2000×10^3 | 12.012 | 0.8000 | 1.1598 | 0.1160 | 0 |
| | 5 | 9.0000×10^3 | 13.146 | 0.8000 | 1.1525 | 0.1152 | 0 |

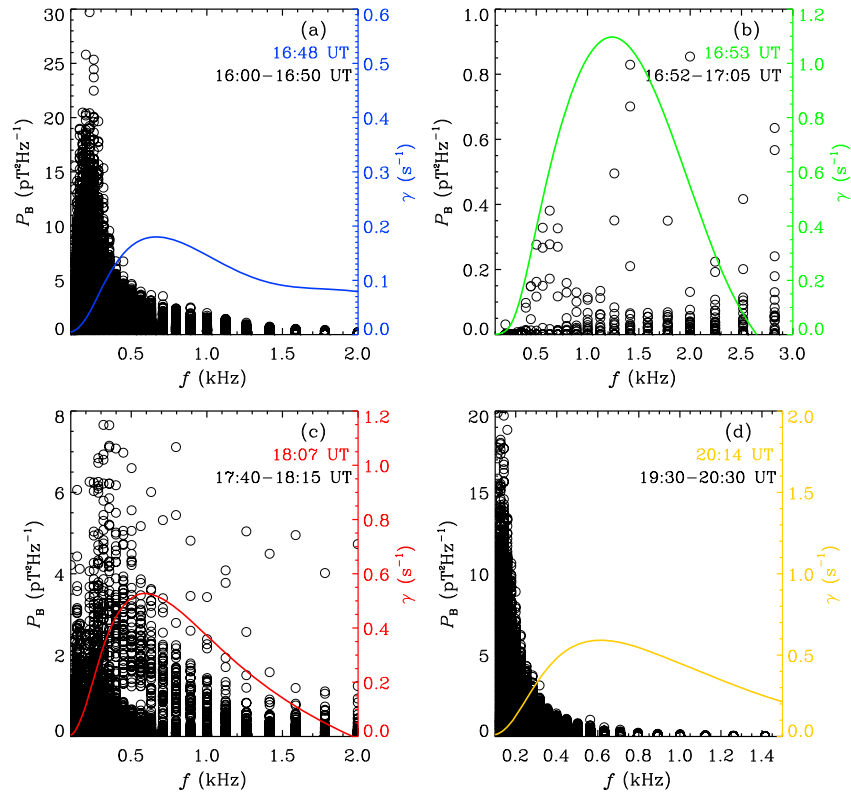


Figure 8. Frequency dependence of wave power spectral intensities (circles) and linear growth rates (lines color coded according to time) during four periods: (a) preshock, (b) postshock, (c) temporary recovery, and (d) substantial recovery.

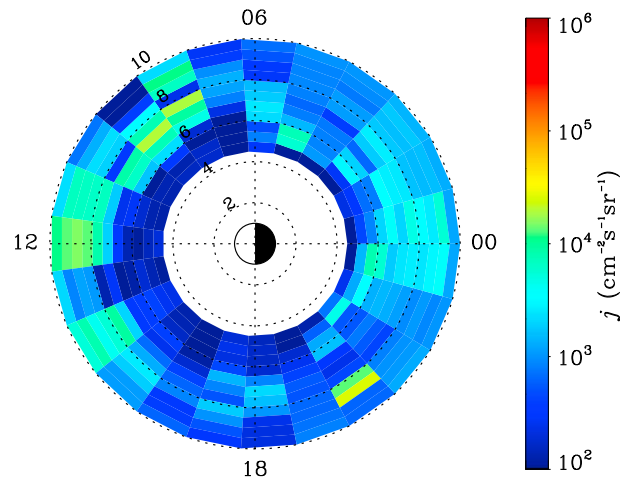


Figure 9. Mean fluxes of the precipitating electrons (40–130 keV) measured by POES satellites from 00:00 UT to 16:00 UT on 27 February 2014.

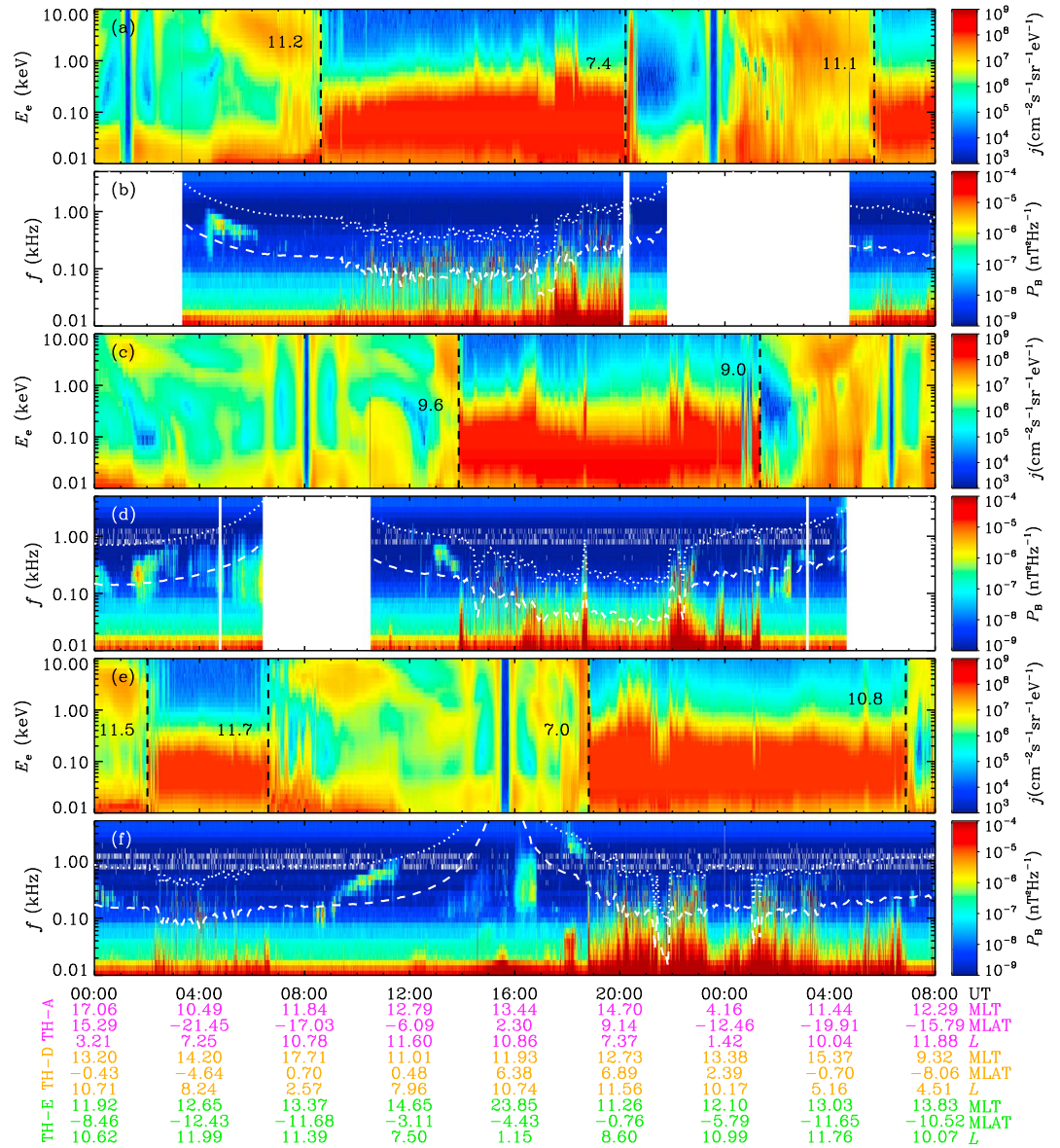


Figure 10. Magnetic field power spectral intensities and electron energy spectrograms measured by (a, b) THEMIS A, (c, d) THEMIS D, and (e, f) THEMIS E satellites. In Figures 10a, 10c, and 10e, the magnetopause locations are marked with dashed lines. In Figures 10b, 10d, and 10f, the dashed and dotted lines represent $0.1f_{ce_eq}$ and $0.5f_{ce_eq}$.

the acceleration/modulation of electrons over a wide energy range. Such phenomenon had been investigated by many researchers in the past (e.g., Blake et al., 1992; Foster et al., 2015; Li et al., 1993; Su et al., 2015; Vampola & Korth, 1992; Zong et al., 2009). Because of the shock acceleration, the hot (tens of keV) electron fluxes increased by up to 10 times and the corresponding temperature anisotropy appeared to be enhanced.

Figure 7 plots the hot electron phase space densities (PSDs) and the local wave growth rates at four specific time moments: (a) preshock moment at 16:48 UT, (b) postshock moment at 16:53 UT, (c) temporary recovery moment at 18:07 UT, and (d) substantial recovery moment at 20:14 UT. At each moment, we fit the observed electron phase space densities (PSDs) with a sum of subtracted Maxwellian components (Ashour-Abdalla & Kennel, 1978; Su et al., 2014):

$$F(v_{\perp}, v_{\parallel}) = \sum_{i=1}^N F_i, \quad (1)$$

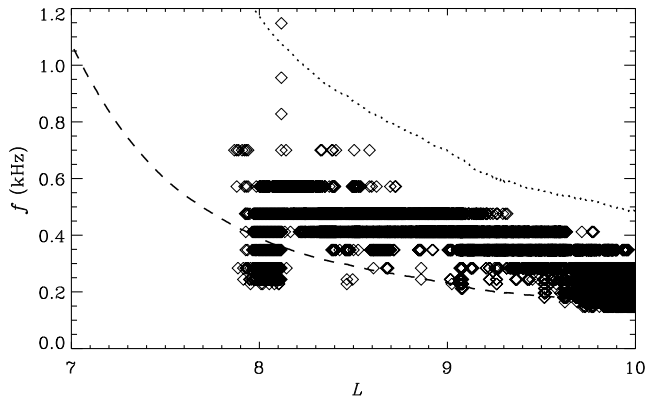


Figure 11. Radial distribution of chorus observed by THEMIS A, THEMIS D, and THEMIS E before the shock. The dashed and dotted lines represent $0.1f_{ce_eq}$ and $0.5f_{ce_eq}$ of THEMIS D from 00:00 UT to 06:00 UT on 27 February 2014.

$$F_i = \frac{n_i}{(\sqrt{\pi}V_{th_i})^3} \exp\left[-\left(\frac{V_{\parallel}}{V_{th_i}} - V_{dr_i}\right)^2\right] \times \left\{ \frac{\Delta_i}{\alpha_{1_i}} \exp\left(-\frac{v_{\perp}^2}{\alpha_{1_i}V_{th_i}^2}\right) + \frac{1 - \Delta_i}{\alpha_{1_i} - \alpha_{2_i}} \times \left[\exp\left(-\frac{v_{\perp}^2}{\alpha_{1_i}V_{th_i}^2}\right) - \exp\left(-\frac{v_{\perp}^2}{\alpha_{2_i}V_{th_i}^2}\right) \right] \right\}. \quad (2)$$

Here the total number of plasma components is referred to as N and the i th component is characterized by the density n_i and the loss cone parameters α_{1_i} , α_{2_i} , and Δ_i . We input these fitting parameters (Table 1) into the Waves in Homogeneous Anisotropic Magnetized Plasma (WHAMP) code (Ronmark, 1982) to calculate the linear growth rates of parallel-propagating whistler-mode waves. The interplanetary shock did not significantly change the growth rates in the core frequency range 0.1–0.5 kHz of plasmaspheric hiss waves. Hence, the disappearance of hiss was unlikely

to be a result of the local process inside the plasmasphere but more likely to be a result of a change of the embryonic source. The postshock growth rates peaked at the frequency ~ 1.2 kHz, roughly explaining the local generation of whistler waves above 1 kHz after the shock. In Figure S1 of the supporting information, we present more examples of the postshock PSDs and the corresponding growth rates. The growth rates in the core frequency range of hiss were always at a low level, and the whistler waves above 1 kHz became almost invisible after 17:10 UT because of the decrease of wave growth rates. During the temporary and substantial recovery periods, the local growth rates were about 2–5 times larger than the preshock values in the core frequency range of hiss waves, indicating the potentially important role of local instability. For the temporarily recovered hiss with the unidirectional Poynting fluxes (Figures 3 and 4), the local instability might be the dominant generation mechanism. After 18:10 UT, because of the increase of minimum resonant energy of hiss waves and the decrease of energetic electron fluxes above 20 keV, the local instability gradually became too weak to produce the observable hiss waves (Figure 5). For the substantially recovered hiss with the bidirectional Poynting fluxes (Figures 3 and 4), both the embryonic source and the local amplification might act at the same time.

Figure 8 compares the frequency distributions between the wave spectra and the corresponding local growth rates in the four previously mentioned periods. During the postshock (Figure 8b) and temporary recovery (Figure 8c) periods, the peak frequencies of wave spectra and the growth rates were quite close to each other, generally supporting the local generation of whistler-mode waves (~ 1.0 kHz after the shock and ~ 0.4 kHz during the temporary recovery period). In contrast, during the preshock (Figure 8a) and substantial recovery (Figure 8d) periods, the wave spectra peaked below 0.3 kHz, obviously deviating from the prediction of local growth. Two plausible explanations may be given for such a deviation. One possibility is the additional contribution of embryonic source (chorus) to the plasmaspheric hiss waves. As described in the next section, one can find the occurrence of <0.3 kHz chorus over a wide spatial region. Another possibility is associated with the nonlinear amplification of plasmaspheric hiss waves (Omura et al., 2015). In the nonlinear frame, the hiss spectrum shape is approximately determined by the frequency profile of the “optimum wave amplitude” for triggering rising or falling tones (Omura et al., 2015).

6. Chorus Distributions and Magnetopause Locations

Figure 9 gives the POES-observed precipitating 40–130 keV electron fluxes to understand the global distribution of chorus waves (Chen, Reeves, et al., 2014; Li, Ni, et al., 2013) before the shock. These electron fluxes have been averaged over the time period of 00:00–16:00 UT on 27 February 2014. In general, the precipitating electron fluxes were at a low level ($j < 3 \times 10^4 \text{ cm}^{-2} \text{ s}^{-1} \text{ sr}^{-1}$) and peaked outside $L = 6$ in the dayside magnetosphere, suggesting the relatively weak strength and the limited occurrence region of the preshock chorus. Figure 10 shows the spatiotemporal characteristics of magnetopause and chorus waves measured locally by THEMIS A, THEMIS D, and THEMIS E in the noonside magnetosphere. The magnetopause is characterized by an abrupt change of the low-energy (<0.3 keV) electron fluxes and the low-frequency (<0.1 kHz)

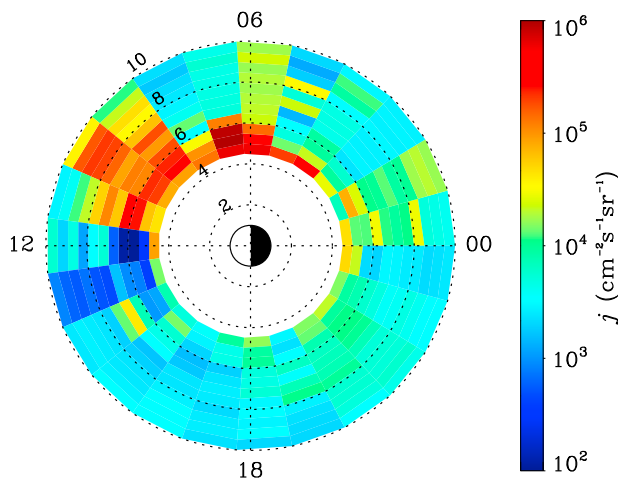


Figure 12. Same as Figure 9, except in the time range from 17:00 UT on 27 February 2014 to 03:00 UT on 28 February 2014.

electromagnetic signals. In the time range of interest, THEMIS A, THEMIS D, and THEMIS E had passed through the magnetopause several times. Before the shock arrival, the subsolar magnetopause was located around $L \sim 10$. The outermost magnetopause ($L = 11.7$) was detected by THEMIS E at 06:37 UT on 27 February, and the innermost magnetopause ($L = 9.6$) was encountered by THEMIS D at 13:52 UT on 27 February. Figure 11 shows the radial distribution of preshock chorus (Figures 10a, 10c, and 10e). The observed chorus waves are found to occur in the dayside plasmatrough from $L = 7.8$ to the magnetopause and have a good correlation with the area of strong precipitating electron fluxes. The chorus frequency range was about $0.1 - 0.3 f_{ce_eq}$ ($0.1 - 0.6$ kHz), covering the core frequency range of preshock hiss. The previous ray-tracing simulations had found that the chorus rays entering the plasmasphere usually had the frequency $0.1 - 0.3 f_{ce_eq}$ (Bortnik et al., 2008; Chen, Bortnik, et al., 2012a). These results imply a potential link between chorus and hiss before the shock. After the shock arrival, the magnetopause was compressed earthward significantly (Figure 1b). The magnetopause moved down to $L = 7.4$ at 18:49 UT (observed by THEMIS A) and $L = 7.0$ at 20:13 UT (observed by THEMIS E) on 27 February. As shown in Figure 11, the earthward moving magne-

topause should promptly eliminate the preexisting dayside chorus waves and the associated source electrons of chorus waves (Figure 1). The quenching of embryonic source (chorus) might be the dominant cause of the plasmaspheric hiss disappearance.

During the substantial recovery of hiss waves, the potential recovery of chorus waves outside $L = 7.0$ was not observed locally by the THEMIS mission because of its limited orbital coverage. Figure 12 presents the POES-observed precipitating electron fluxes in the time period from 17:00 UT on 27 February 2014 to 03:00 UT on 28 February 2014. As a result of the significant injection of hot electrons during the prolonged substorms (Figures 2b and 5), the precipitating electron fluxes were intensified significantly. Outside $L = 7.0$, the peak of precipitating electron fluxes was located in the range of MLT = 9–12 (similar to the situation reported by Meredith et al. (2011)), and the corresponding chorus (Figure 1b) could serve as the embryonic source of the substantially recovered hiss waves in the postnoon sector (MLT = 13–14). As shown in the previous ray-tracing simulations in a magnetospheric environment containing a plasmaspheric plume (Chen et al., 2009), the prenoon chorus can propagate into the plasmasphere and contribute to the plasmaspheric hiss waves over a broad MLT range. The off-meridian propagation and the multiple magnetosphere reflections of rays might explain the observed low planarity of hiss waves (Figures 3 and 4). In contrast, the preshock hiss waves were observed roughly in the same MLT sector as the embryonic source. These waves possessed the relatively large planarity values (Figures 3 and 4) probably without experiencing too many magnetospheric reflections.

7. Discussions and Conclusions

Plasmaspheric hiss is an important whistler-mode emission controlling the evolution of the radiation belt electrons, whose generation mechanism remains under debate. In the past, excitation by electron cyclotron instability in the outer plasmasphere (Thorne et al., 1979) and origination from chorus outside the plasmasphere (Bortnik et al., 2008, 2009) have been proposed as two leading paradigms. In this study, on the basis of multipoint observations from RBSP, THEMIS, and POES satellites, we attempt to determine the dominant mechanisms for the shock-induced disappearance and subsequent recovery of plasmaspheric hiss on 27 February 2014. The principal conclusions are summarized as follows:

1. Before the shock, the hot electron fluxes inside the plasmasphere and the internal amplification of waves were quite weak. The dayside chorus waves outside $L \simeq 7$ were identified as the dominant source of plasmaspheric hiss with the bidirectional Poynting fluxes. Following the shock compression, the subsolar magnetopause shrank from $10 R_E$ to about $7 R_E$ and the preexisting chorus waves and their source electrons were promptly removed. At the same time, although the shock increased the electron fluxes below 50 keV in the plasmasphere, there was no significant enhancement of the local growth rates in the core frequency range of plasmaspheric hiss (primarily because of the increase of local magnetic field and the minimum resonant energy). The quenching of embryonic source and the insignificant variation of internal amplification led to the disappearance of plasmaspheric hiss after the shock.

2. As time went on, a lot of hot electrons were injected into the inner magnetosphere by the intense substorms. Both the temporary and substantial recoveries of plasmaspheric hiss were closely related to the significant enhancement of hot electron fluxes. The local growth rates in the core frequency range of plasmaspheric hiss became 2–5 times larger than the preshock values. For the temporarily recovered hiss with unidirectional Poynting fluxes, the local instability of hot electrons was likely to be the dominant generation mechanism. In contrast, both the embryonic source (chorus) in the prenoon sector and the enhanced internal amplification could contribute to the substantially recovered plasmaspheric hiss with bidirectional Poynting fluxes.

In this study, to qualitatively evaluate the role of internal instability in the generation of plasmaspheric hiss, we calculate the local growth rates of whistler waves based on the linear instability theory (Kennel & Petschek, 1966). The magnetospheric plasma is often marginally stable with respect to the whistler-mode wave generation. The WHAMP modeling here only provides an approximate understanding of the whistler-mode wave instability and may not capture some subtle changes in electron distributions which could affect the wave amplification/excitation. In the future, the underlying nonlinear cyclotron resonance process (Omura et al., 2015) should be investigated to better understand the amplification/excitation of waves inside the plasmasphere. Also, future ray-tracing simulations including the event-specific magnetospheric environment parameters (e.g., Chen et al., 2009) are required to examine the conclusions drawn here.

Acknowledgments

This work was supported by the National Natural Science Foundation of China grants 41631071, 41422405, 41274169, 41274174, 41174125, 41131065, 41421063, 41231066, and 41304134, the Chinese Academy of Sciences grants KZCX2-EW-QN510 and KZZD-EW-01-4, the CAS Key Research Program of Frontier Sciences grant QYZDB-SSW-DQC015, the National Key Basic Research Special Foundation of China grant 2011CB811403, and the Fundamental Research Funds for the Central Universities WK2080000077. We acknowledge J. H. King, N. Papatashvili, and CDAWeb for the use of interplanetary parameters and magnetospheric indices; acknowledge the University of Iowa as the source for the EMFISIS data (this acknowledgment does not imply endorsement of the publication by the University of Iowa or its researchers); and acknowledge THEMIS team for the use of SCM, FGM, ESA, SST, and EFI data. The interplanetary parameters and geomagnetic indices are obtained at the CDAWeb (http://cdaweb.gsfc.nasa.gov/cdaweb/istp_public/). The RBSP data are available at the websites <http://emfis. physics.uiowa.edu/Flight/> for EMFISIS, http://www.rbsp-ect.lanl.gov/data_pub/ for ECT, and <http://www.space.umn.edu/rbspfwh-data/> for EFW. The THEMIS data are available at the website <http://themis.ssl.berkeley.edu/data/themis/>.

References

- Abel, B., & Thorne, R. M. (1998). Electron scattering loss in Earth's inner magnetosphere 1. Dominant physical processes. *Journal of Geophysical Research*, *103*, 2385–2396. <https://doi.org/10.1029/97JA02919>
- Albert, J. M. (1994). Quasi-linear pitch angle diffusion coefficients: Retaining high harmonics. *Journal of Geophysical Research*, *99*, 23,741–23,745. <https://doi.org/10.1029/94JA02345>
- Angelopoulos, V. (2008). The THEMIS mission. *Space Science Reviews*, *141*, 5–34. <https://doi.org/10.1007/s11214-008-9336-1>
- Ashour-Abdalla, M., & Kennel, C. F. (1978). Nonconvective and convective electron cyclotron harmonic instabilities. *Journal of Geophysical Research*, *83*, 1531–1543. <https://doi.org/10.1029/JA083iA04p01531>
- Auster, H. U., Glassmeier, K. H., Magnes, W., Aydogar, O., Baumjohann, W., Constantinescu, D., ... Wiedemann, M. (2008). The THEMIS Fluxgate Magnetometer. *Space Science Reviews*, *141*, 235–264. <https://doi.org/10.1007/s11214-008-9365-9>
- Blake, J. B., Carranza, P. A., Claudepierre, S. G., Clemmons, J. H., Crain, W. R., Dotan, Y., ... Zakrzewski, M. P. (2013). The magnetic electron ion spectrometer (MagEIS) instruments aboard the Radiation Belt Storm Probes (RBSP) spacecraft. *Space Science Reviews*, *179*, 383–421. <https://doi.org/10.1007/s11214-013-9991-8>
- Blake, J. B., Kolasinski, W. A., Fillius, R. W., & Mullen, E. G. (1992). Injection of electrons and protons with energies of tens of MeV into *L* less than 3 on 24 March 1991. *Geophysical Research Letters*, *19*, 821–824. <https://doi.org/10.1029/92GL00624>
- Bonnell, J. W., Mozer, F. S., Delory, G. T., Hull, A. J., Ergun, R. E., Cully, C. M., ... Harvey, P. R. (2008). The Electric Field Instrument (EFI) for THEMIS. *Space Science Reviews*, *141*, 303–341. <https://doi.org/10.1007/s11214-008-9469-2>
- Bortnik, J., Chen, L., Li, W., Thorne, R. M., & Horne, R. B. (2011). Modeling the evolution of chorus waves into plasmaspheric hiss. *Journal of Geophysical Research*, *116*, A08221. <https://doi.org/10.1029/2011JA016499>
- Bortnik, J., Chen, L., Li, W., Thorne, R. M., Meredith, N. P., & Horne, R. B. (2011). Modeling the wave power distribution and characteristics of plasmaspheric hiss. *Journal of Geophysical Research*, *116*, A12209. <https://doi.org/10.1029/2011JA016862>
- Bortnik, J., Li, W., Thorne, R. M., Angelopoulos, V., Cully, C., Bonnell, J., ... Roux, A. (2009). An observation linking the origin of plasmaspheric hiss to discrete chorus emissions. *Science*, *324*, 775–778. <https://doi.org/10.1126/science.1171273>
- Bortnik, J., Thorne, R. M., & Meredith, N. P. (2008). The unexpected origin of plasmaspheric hiss from discrete chorus emissions. *Nature*, *452*, 62–66. <https://doi.org/10.1038/nature06741>
- Chen, L., Bortnik, J., Li, W., Thorne, R. M., & Horne, R. B. (2012a). Modeling the properties of plasmaspheric hiss: 1. Dependence on chorus wave emission. *Journal of Geophysical Research*, *117*, A05201. <https://doi.org/10.1029/2011JA017201>
- Chen, L., Bortnik, J., Li, W., Thorne, R. M., & Horne, R. B. (2012b). Modeling the properties of plasmaspheric hiss: 2. Dependence on the plasma density distribution. *Journal of Geophysical Research*, *117*, A05202. <https://doi.org/10.1029/2011JA017202>
- Chen, L., Bortnik, J., Thorne, R. M., Horne, R. B., & Jordanova, V. K. (2009). Three-dimensional ray tracing of VLF waves in a magnetospheric environment containing a plasmaspheric plume. *Geophysical Research Letters*, *36*, L22101. <https://doi.org/10.1029/2009GL040451>
- Chen, L., Li, W., Bortnik, J., & Thorne, R. M. (2012). Amplification of whistler-mode hiss inside the plasmasphere. *Geophysical Research Letters*, *39*, L08111. <https://doi.org/10.1029/2012GL051488>
- Chen, L., Thorne, R. M., Bortnik, J., Li, W., Horne, R. B., Reeves, G. D., ... Fennell, J. F. (2014). Generation of unusually low frequency plasmaspheric hiss. *Geophysical Research Letters*, *41*, 5702–5709. <https://doi.org/10.1002/2014GL060628>
- Chen, Y., Reeves, G. D., Friedel, R. H. W., & Cunningham, G. S. (2014). Global time-dependent chorus maps from low-Earth-orbit electron precipitation and Van Allen Probes data. *Geophysical Research Letters*, *41*, 755–761. <https://doi.org/10.1002/2013GL059181>
- Church, S. R., & Thorne, R. M. (1983). On the origin of plasmaspheric hiss—Ray path integrated amplification. *Journal of Geophysical Research*, *88*, 7941–7957. <https://doi.org/10.1029/JA088iA10p07941>
- Cornilleau-Wehrlin, N., Solomon, J., Korth, A., & Kremser, G. (1993). Generation mechanism of plasmaspheric ELF/VLF hiss: A statistical study from GEOS 1 data. *Journal of Geophysical Research*, *98*, 21,471–21,480. <https://doi.org/10.1029/93JA01919>
- Cornwall, J. M. (1964). Scattering of energetic trapped electrons by very-low-frequency waves. *Journal of Geophysical Research*, *69*, 1251–1258. <https://doi.org/10.1029/JZ069i007p01251>
- Dittberner, G. (2002). GOES, POES, NPOESS—Plans for America's civil operational environmental satellite programs, *34th COSPAR Scientific Assembly* (Vol. 34). Houston, TX: The Second World Space Congress, COSPAR Meeting.
- Draganov, A. B., Inan, U. S., Sonwalkar, V. S., & Bell, T. F. (1992). Magnetically reflected whistlers as a source of plasmaspheric hiss. *Geophysical Research Letters*, *19*, 233–236. <https://doi.org/10.1029/91GL03167>

- Foster, J. C., Wygant, J. R., Hudson, M. K., Boyd, A. J., Baker, D. N., Erickson, P. J., & Spence, H. E. (2015). Shock-induced prompt relativistic electron acceleration in the inner magnetosphere. *Journal of Geophysical Research: Space Physics*, *120*, 1661–1674. <https://doi.org/10.1002/2014JA020642>
- Funsten, H. O., Skoug, R. M., Guthrie, A. A., MacDonald, E. A., Baldonado, J. R., Harper, R. W., ... Chen, J. (2013). Helium, Oxygen, Proton, and Electron (HOPE) mass spectrometer for the Radiation Belt Storm Probes mission. *Space Science Reviews*, *179*, 423–484. <https://doi.org/10.1007/s11214-013-9968-7>
- Goldstein, J., Pascuale, S. D., Kletzing, C., Kurth, W., Genestreti, K. J., Skoug, R. M., ... Spence, H. (2014). Simulation of Van Allen Probes plasmopause encounters. *Journal of Geophysical Research: Space Physics*, *119*, 7464–7484. <https://doi.org/10.1002/2014JA020252>
- Green, J. L., Boardsen, S., Garcia, L., Taylor, W. W. L., Fung, S. F., & Reinisch, B. W. (2005). On the origin of whistler mode radiation in the plasmasphere. *Journal of Geophysical Research*, *110*, A03201. <https://doi.org/10.1029/2004JA010495>
- Hayakawa, M., & Sazhin, S. S. (1992). Mid-latitude and plasmaspheric hiss—A review. *Planetary and Space Science*, *40*, 1325–1338. [https://doi.org/10.1016/0032-0633\(92\)90089-7](https://doi.org/10.1016/0032-0633(92)90089-7)
- He, Z., Yan, Q., Chu, Y., & Cao, Y. (2016). Wave-driven gradual loss of energetic electrons in the slot region. *Journal of Geophysical Research: Space Physics*, *121*, 8614–8623. <https://doi.org/10.1002/2016JA023087>
- Horne, R. B., & Thorne, R. M. (1998). Potential waves for relativistic electron scattering and stochastic acceleration during magnetic storms. *Geophysical Research Letters*, *25*, 3011–3014. <https://doi.org/10.1029/98GL01002>
- Huang, C. Y., Goertz, C. K., & Anderson, R. R. (1983). A theoretical study of plasmaspheric hiss generation. *Journal of Geophysical Research*, *88*, 7927–7940. <https://doi.org/10.1029/JA088iA10p07927>
- Kennel, C. F., & Petschek, H. E. (1966). Limit on stably trapped particle fluxes. *Journal of Geophysical Research*, *71*, 1–28. <https://doi.org/10.1029/JZ071i001p00001>
- King, J. H., & Papitashvili, N. E. (2005). Solar wind spatial scales in and comparisons of hourly Wind and ACE plasma and magnetic field data. *Journal of Geophysical Research*, *110*, A02104. <https://doi.org/10.1029/2004JA010649>
- Kletzing, C. A., Kurth, W. S., Acuna, M., MacDowall, R. J., Torbert, R. B., Averkamp, T., ... Tyler, J. (2013). The Electric and Magnetic Field Instrument Suite and Integrated Science (EMFISIS) on RBSP. *Space Science Reviews*, *179*, 127–181. <https://doi.org/10.1007/s11214-013-9993-6>
- Kletzing, C., Kurth, W. S., Bounds, S. R., Hospodarsky, G. B., Santolik, O., Wygant, J. R., ... Summers, D. (2014). Evidence for significant local generation of plasmaspheric hiss. Abstract SM14A-09 Presented at the 2014 AGU Fall Meeting, San Francisco, CA, 15–19 Dec.
- Laakso, H., Santolik, O., Horne, R., Kolmasová, I., Escoubet, P., Masson, A., & Taylor, M. (2015). Identifying the source region of plasmaspheric hiss. *Geophysical Research Letters*, *42*, 3141–3149. <https://doi.org/10.1002/2015GL063755>
- Lam, M. M., Horne, R. B., Meredith, N. P., Glauert, S. A., Moffat-Griffin, T., & Green, J. C. (2010). Origin of energetic electron precipitation >30 keV into the atmosphere. *Journal of Geophysical Research*, *115*, A00F08. <https://doi.org/10.1029/2009JA014619>
- Le Contel, O., Roux, A., Robert, P., Coillot, C., Bouabdellah, A., de La Porte, B., ... Larson, D. (2008). First results of the THEMIS Search Coil Magnetometers. *Space Science Reviews*, *141*, 509–534. <https://doi.org/10.1007/s11214-008-9371-y>
- Li, W., Chen, L., Bortnik, J., Thorne, R. M., Angelopoulos, V., Kletzing, C. A., ... Hospodarsky, G. B. (2015). First evidence for chorus at a large geocentric distance as a source of plasmaspheric hiss: Coordinated THEMIS and Van Allen Probes observation. *Geophysical Research Letters*, *42*, 241–248. <https://doi.org/10.1002/2014GL02832>
- Li, W., Ni, B., Thorne, R. M., Bortnik, J., Green, J. C., Kletzing, C. A., ... Hospodarsky, G. B. (2013). Constructing the global distribution of chorus wave intensity using measurements of electrons by the POES satellites and waves by the Van Allen Probes. *Geophysical Research Letters*, *40*, 4526–4532. <https://doi.org/10.1002/grl.50920>
- Li, W., Shprits, Y. Y., & Thorne, R. M. (2007). Dynamic evolution of energetic outer zone electrons due to wave-particle interactions during storms. *Journal of Geophysical Research*, *112*, A10220. <https://doi.org/10.1029/2007JA012368>
- Li, W., Thorne, R. M., Bortnik, J., Nishimura, Y., Angelopoulos, V., Chen, L., ... Bonnell, J. W. (2010). Global distributions of suprathermal electrons observed on THEMIS and potential mechanisms for access into the plasmasphere. *Journal of Geophysical Research*, *115*, A00J10. <https://doi.org/10.1029/2010JA015687>
- Li, W., Thorne, R. M., Bortnik, J., Reeves, G. D., Kletzing, C. A., Kurth, W. S., ... Thaller, S. A. (2013). An unusual enhancement of low-frequency plasmaspheric hiss in the outer plasmasphere associated with substorm-injected electrons. *Geophysical Research Letters*, *40*, 3798–3803. <https://doi.org/10.1002/grl.50787>
- Li, X., Roth, I., Temerin, M., Wygant, J. R., Hudson, M. K., & Blake, J. B. (1993). Simulation of the prompt energization and transport of radiation belt particles during the March 24, 1991 SSC. *Geophysical Research Letters*, *20*, 2423–2426. <https://doi.org/10.1029/93GL02701>
- Lin, R. L., Zhang, X. X., Liu, S. Q., Wang, Y. L., & Gong, J. C. (2010). A three-dimensional asymmetric magnetopause model. *Journal of Geophysical Research*, *115*, A04207. <https://doi.org/10.1029/2009JA014235>
- Liu, N., Su, Z., Gao, Z., Zheng, H., Wang, Y., Wang, S., ... Wygant, J. R. (2017). Simultaneous disappearances of plasmaspheric hiss, exohiss, and chorus waves triggered by a sudden decrease in solar wind dynamic pressure. *Geophysical Research Letters*, *44*, 52–61. <https://doi.org/10.1002/2016GL071987>
- Lyons, L. R., & Thorne, R. M. (1973). Equilibrium structure of radiation belt electrons. *Journal of Geophysical Research*, *78*, 2142–2149. <https://doi.org/10.1029/JA078i013p02142>
- Mauk, B. H., Fox, N. J., Kanekal, S. G., Kessel, R. L., Sibeck, D. G., & Ukhorskiy, A. (2013). Science objectives and rationale for the Radiation Belt Storm Probes mission. *Space Science Reviews*, *179*, 3–27. <https://doi.org/10.1007/s11214-012-9908-y>
- McFadden, J. P., Carlson, C. W., Larson, D., Bonnell, J., Mozer, F., Angelopoulos, V., ... Auster, U. (2008). THEMIS ESA first science results and performance issues. *Space Science Reviews*, *141*, 477–508. <https://doi.org/10.1007/s11214-008-9433-1>
- Meredith, N. P., Horne, R. B., Bortnik, J., Thorne, R. M., Chen, L., Li, W., & Sicard-Piet, A. (2013). Global statistical evidence for chorus as the embryonic source of plasmaspheric hiss. *Geophysical Research Letters*, *40*, 2891–2896. <https://doi.org/10.1002/grl.50593>
- Meredith, N. P., Horne, R. B., Glauert, S. A., & Anderson, R. R. (2007). Slot region electron loss timescales due to plasmaspheric hiss and lightning-generated whistlers. *Journal of Geophysical Research*, *112*, 8214. <https://doi.org/10.1029/2007JA012413>
- Meredith, N. P., Horne, R. B., Lam, M. M., Denton, M. H., Borovsky, J. E., & Green, J. C. (2011). Energetic electron precipitation during high-speed solar wind stream driven storms. *Journal of Geophysical Research*, *116*, A05223. <https://doi.org/10.1029/2010JA016293>
- Meredith, N. P., Horne, R. B., Thorne, R. M., Summers, D., & Anderson, R. R. (2004). Substorm dependence of plasmaspheric hiss. *Journal of Geophysical Research*, *109*, A06209. <https://doi.org/10.1029/2004JA010387>
- Mourenas, D., & Ripoll, J.-F. (2012). Analytical estimates of quasi-linear diffusion coefficients and electron lifetimes in the inner radiation belt. *Journal of Geophysical Research*, *117*, A01204. <https://doi.org/10.1029/2011JA016985>
- Ni, B., Li, W., Thorne, R. M., Bortnik, J., Ma, Q., Chen, L., ... Claudepierre, S. G. (2014). Resonant scattering of energetic electrons by unusual low-frequency hiss. *Geophysical Research Letters*, *41*, 1854–1861. <https://doi.org/10.1002/2014GL059389>

- Omura, Y., Nakamura, S., Kletzing, C. A., Summers, D., & Hikishima, M. (2015). Nonlinear wave growth theory of coherent hiss emissions in the plasmasphere. *Journal of Geophysical Research: Space Physics*, *120*, 7642–7657. <https://doi.org/10.1002/2015JA021520>
- Ronnmark, K. (1982). Waves in homogeneous, anisotropic, multicomponent plasmas (Technical Report No. 179, 55 p.). Kiruna Sweden: Kiruna Geophysical Institute.
- Russell, C. T., Holzer, R. E., & Smith, E. J. (1969). OGO 3 observations of ELF noise in the magnetosphere. 1. Spatial extent and frequency of occurrence. *Journal of Geophysical Research*, *74*, 755–777. <https://doi.org/10.1029/JA074i003p00755>
- Santolik, O., Macušová, E., Kolmašová, I., Cornilleau-Wehrlin, N., & Conchy, Y. (2014). Propagation of lower-band whistler-mode waves in the outer Van Allen belt: Systematic analysis of 11 years of multi-component data from the Cluster spacecraft. *Geophysical Research Letters*, *41*, 2729–2737. <https://doi.org/10.1002/2014GL059815>
- Santolik, O., Parrot, M., & Lefeuvre, F. (2003). Singular value decomposition methods for wave propagation analysis. *Radio Science*, *38*(1), 1010. <https://doi.org/10.1029/2000RS002523>
- Shprits, Y. Y., Subbotin, D., & Ni, B. (2009). Evolution of electron fluxes in the outer radiation belt computed with the VERB code. *Journal of Geophysical Research*, *114*, A11209. <https://doi.org/10.1029/2008JA013784>
- Solomon, J., Cornilleau-Wehrlin, N., Korth, A., & Kremser, G. (1988). An experimental study of ELF/VLF hiss generation in the Earth's magnetosphere. *Journal of Geophysical Research*, *93*, 1839–1847. <https://doi.org/10.1029/JA093iA03p01839>
- Sonwalkar, V. S., & Inan, U. S. (1989). Lightning as an embryonic source of VLF hiss. *Journal of Geophysical Research*, *94*, 6986–6994. <https://doi.org/10.1029/JA094iA06p06986>
- Spence, H. E., Reeves, G. D., Baker, D. N., Blake, J. B., Bolton, M., Bourdarie, S., ... Thorne, R. M. (2013). Science goals and overview of the energetic particle, composition, and thermal plasma (ECT) suite on NASA's Radiation Belt Storm Probes (RBSP) mission. *Space Science Reviews*, *179*, 311–336. <https://doi.org/10.1007/s11214-013-0007-5>
- Stix, T. H. (1962). *The theory of plasma waves*. New York: McGraw-Hill.
- Su, Z., Gao, Z., Zhu, H., Li, W., Zheng, H., Wang, Y., ... Wygant, J. R. (2016). Nonstorm time dropout of radiation belt electron fluxes on 24 September 2013. *Journal of Geophysical Research: Space Physics*, *121*, 6400–6416. <https://doi.org/10.1002/2016JA022546>
- Su, Z., Xiao, F., Zheng, H., & Wang, S. (2011). CRRES observation and STEERB simulation of the 9 October 1990 electron radiation belt dropout event. *Geophysical Research Letters*, *38*, L06106. <https://doi.org/10.1029/2011GL046873>
- Su, Z., Zhu, H., Xiao, F., Zheng, H., Wang, Y., He, Z., ... Wygant, J. R. (2014). Intense duskside lower band chorus waves observed by Van Allen Probes: Generation and potential acceleration effect on radiation belt electrons. *Journal of Geophysical Research: Space Physics*, *119*, 4266–4273. <https://doi.org/10.1002/2014JA019919>
- Su, Z., Zhu, H., Xiao, F., Zheng, H., Wang, Y., Shen, C., ... Wygant, J. R. (2015). Disappearance of plasmaspheric hiss following interplanetary shock. *Geophysical Research Letters*, *42*, 3129–3140. <https://doi.org/10.1002/2015GL063906>
- Summers, D., Ni, B., & Meredith, N. P. (2007). Timescales for radiation belt electron acceleration and loss due to resonant wave-particle interactions: 1. Theory. *Journal of Geophysical Research*, *112*, A04206. <https://doi.org/10.1029/2006JA011801>
- Summers, D., Ni, B., Meredith, N. P., Horne, R. B., Thorne, R. M., Moldwin, M. B., & Anderson, R. R. (2008). Electron scattering by whistler-mode ELF hiss in plasmaspheric plumes. *Journal of Geophysical Research*, *113*, A04219. <https://doi.org/10.1029/2007JA012678>
- Summers, D., Omura, Y., Nakamura, S., & Kletzing, C. A. (2014). Fine structure of plasmaspheric hiss. *Journal of Geophysical Research: Space Physics*, *119*, 9134–9149. <https://doi.org/10.1002/2014JA020437>
- Summers, D., Thorne, R. M., & Xiao, F. (1998). Relativistic theory of wave-particle resonant diffusion with application to electron acceleration in the magnetosphere. *Journal of Geophysical Research*, *103*, 20,487–20,500. <https://doi.org/10.1029/98JA01740>
- Thébault, E., Finlay, C. C., Beggan, C. D., Alken, P., Aubert, J., Barrois, O., ... Zvereva, T. (2015). International Geomagnetic Reference Field: The 12th generation. *Earth, Planets, and Space*, *67*(1), 1–19. <https://doi.org/10.1186/s40623-015-0228-9>
- Thorne, R. M., Church, S. R., & Gorney, D. J. (1979). On the origin of plasmaspheric hiss—The importance of wave propagation and the plasmopause. *Journal of Geophysical Research*, *84*, 5241–5247. <https://doi.org/10.1029/JA084iA09p05241>
- Thorne, R. M., Li, W., Ni, B., Ma, Q., Bortnik, J., Baker, D. N., ... Angelopoulos, V. (2013). Evolution and slow decay of an unusual narrow ring of relativistic electrons near $L \sim 3.2$ following the september 2012 magnetic storm. *Geophysical Research Letters*, *40*, 3507–3511. <https://doi.org/10.1002/grl.50627>
- Thorne, R. M., Smith, E. J., Burton, R. K., & Holzer, R. E. (1973). Plasmaspheric hiss. *Journal of Geophysical Research*, *78*, 1581–1596. <https://doi.org/10.1029/JA078i010p01581>
- Tsyganenko, N. A., & Sitnov, M. I. (2005). Modeling the dynamics of the inner magnetosphere during strong geomagnetic storms. *Journal of Geophysical Research*, *110*, A03208. <https://doi.org/10.1029/2004JA010798>
- Vampola, A. L., & Korth, A. (1992). Electron drift echoes in the inner magnetosphere. *Geophysical Research Letters*, *19*, 625–628. <https://doi.org/10.1029/92GL00121>
- Wygant, J., Bonnell, J., Goetz, K., Ergun, R., Mozer, F., Bale, S., ... Tao, J. (2013). The electric field and waves instruments on the radiation belt storm probes mission. *Space Science Reviews*, *179*(1–4), 183–220. <https://doi.org/10.1007/s11214-013-0013-7>
- Zong, Q., Zhou, X., Wang, Y. F., Li, X., Song, P., Baker, D. N., ... Pedersen, A. (2009). Energetic electron response to ULF waves induced by interplanetary shocks in the outer radiation belt. *Journal of Geophysical Research*, *114*, A10204. <https://doi.org/10.1029/2009JA014393>